Letter

Radio-Frequency Coulomb-Blockade Thermometry

Florian Blanchet,* Yu-Cheng Chang, Bayan Karimi, Joonas T. Peltonen, and Jukka P. Pekola†
Pico group, QTF Centre of Excellence, Department of Applied Physics, Aalto University, P.O. Box 15100, Aalto FI-00076, Finland

(Received 24 September 2021; revised 19 November 2021; accepted 10 December 2021; published 26 January 2022)

We present a scheme and demonstrate measurements of a Coulomb-blockade thermometer (CBT) in a microwave-transmission setup. The sensor is embedded in an *LCR* resonator, where R is determined by the conductance of the junction array of the CBT. A transmission measurement yields a signal that is directly proportional to the conductance of the CBT, thus enabling the calibration-free operation of the thermometer. This is verified by measuring an identical sensor simultaneously in the usual dc setup. The important advantage of the rf measurement is its speed: the whole bias dependence of the CBT conductance can now be measured in a time of about 100 ms, which is 1000 times faster than in a standard dc measurement. The achieved noise-equivalent temperature of this rf primary measurement is about 1 mK/$\sqrt{\text{Hz}}$ at the bath temperature $T = 200$ mK.

DOI: 10.1103/PhysRevApplied.17.L011003

I. INTRODUCTION

Traditional single-electron tunneling phenomena are present when the temperature T is much lower than the unit of capacitive charging energy E_C that determines the energy cost of adding or removing an electron in the device [1,2]. In this Coulomb-blockade regime, $k_BT \ll E_C$, the charge transport is independent of the temperature. Yet in the opposite regime, $k_BT \gtrsim E_C$, one obtains a thermometer with attractive properties [3–7]. A Coulomb-blockade thermometer (CBT) is typically formed of an array of tunnel junctions and it provides calibration-free (primary) thermometry in its operation range, the temperature being deduced from a simple conductance measurement. Up to the present day, CBTs have been used as reliable thermometers in the temperature range from 200 μK up to 60 K [8–13] and in magnetic fields up to 27 T [14,23]. To have a measure of absolute temperature, one needs to map the whole dependence of the differential conductance at bias-voltage values ranging over several k_BT/e. This is straightforward but in standard dc or quasi-dc measurements, it typically takes several minutes in order to reach satisfactory accuracy in thermometry. Another option to measure the conductance is to monitor either the reflectance or the conductance in a resonant circuit, with the device under study embedded [15–18]. In this letter, we propose and demonstrate experimentally an rf transmission measurement of a CBT, where similar accuracy is achieved in less than 1 s. The transmitted microwave power is related to the conductance in a simple linear way, making the analysis and the determination of temperature from the measured signal straightforward.

II. BASICS OF THE THERMOMETER OPERATION

When one measures the current (I) and voltage across the array (V) characteristics of a uniform series of N tunnel junctions with normal metal electrodes, the asymptotic slope, i.e., the conductance G of this curve, at $|eV/N| \gg k_BT, E_C$, is given by $G_T \equiv R_\Sigma^{-1}$, where R_Σ is the total series resistance of the junctions and V is the voltage across the whole array of junctions [see Fig. 1(a)]. At lower voltages, Coulomb repulsion of electrons on the islands lowers the conductance such that there is either full suppression of G at $|eV/N| \lesssim E_C$ at $k_BT \ll E_C$ or partial suppression at $|eV/N| \lesssim k_BT$ for $k_BT \gtrsim E_C$, i.e., in the CBT operation range. Quantitatively, for $k_BT \gtrsim E_C$, the dependence of the conductance on the bias voltage can be cast in a universal form [4]

$$G(v)/G_T = 1 - u\,g(v) - \frac{u^2}{4}[g'(v)h'(v) + g''(v)h(v)], \qquad (1)$$

where $g(v) = e^v[e^v(v-2)+v+2]/(e^v-1)^3$, $u = E_C/(k_BT)$, $v = eV/(Nk_BT)$, and $h(v) = v\coth(v/2)$. The charging energy E_C is given by the full capacitance matrix of the thermometer; for an array with junction capacitance C for each of them and vanishing stray capacitance, $E_C = (1-1/N)e^2/C$. The important property of Eq. (1) is that measuring the voltage half width at full minimum, $V_{1/2}$, gives the absolute temperature without the need to

*florian.blanchet@aalto.fi
†jukka.pekola@aalto.fi

know the specific parameters of the sensor apart from the number of junctions in the array. The commonly adopted result valid for $u \ll 1$ [the first line of Eq. (1)] tells us that $V_{1/2} = 5.4392 N k_B T/e$, i.e.,

$$T = 0.18\,385 \frac{e}{N k_B} V_{1/2}. \tag{2}$$

The numerical prefactor arises from the functional form of $g(x)$. The depth of the zero-bias dip, $\Delta G \equiv G_T - G(0)$, can also serve as a thermometer, since $\Delta G/G_T \approx u/6$, (again up to linear order in u) but here the calibration depends on the capacitances via E_C (secondary thermometer). The corrections to Eq. (2) arising from the second line in Eq. (1) lead to [4]

$$T = 0.18\,385 \frac{e}{N k_B} V_{1/2}/(1 + 0.3921 \Delta G/G_T), \tag{3}$$

where the correction, $(1 + 0.3921 \Delta G/G_T)^{-1}$, can be easily determined from the measured depth $\Delta G/G_T$. This correction is about 2% in T at the lowest temperatures of the current measurement and smaller above it. Equations (1)–(3) are naturally valid only for a uniform array; corrections due to nonuniformities are discussed, e.g., in Ref. [4].

III. rf MEASUREMENT

The actual sample and the measurement setup are presented schematically in Figs. 1(a) and 1(b), together with the full wiring, amplifiers, and attenuators in Fig. 1(c). The heart of the system is an *LCR* tank circuit that resonates at $f_0 \approx 547$ MHz. The CBT thermometer forms the parallel dissipation R of this resonator. The *LC* is formed of a superconducting (Nb) spiral. With the actual component values, $L = 110$ nH, $C = 540$ fF, and $R \approx R_\Sigma = 80$ kΩ as the resistance of 80 junctions in series in eight parallel chains [sample CBT80, shown in Fig. 1(a)] to be described below. The quality factor of the resonator is $Q \approx 45$. This yields an internal response time of the measurement as $Q/(2\pi f_0) \sim 13$ ns, which is far shorter than the typical data-acquisition times in this work. The measured signal is the transmission from rf in to rf out [see Figs. 1(a) and 1(b)], through the coupling capacitances $C_1 \approx 67$ fF and $C_2 \approx 170$ fF at the input and output, respectively. These values are obtained from SONNET simulation and are also consistent with the mutual capacitance matrix simulated by COMSOL. This transmission is affected by the differential conductance of the CBT sensor, which is placed physically on a different chip, next to the one with the resonator. The dc bias voltage V is applied via the bias tee [shown in Figs. 1(a) and 1(b)], where the inductor is formed by another spiral filter made of Nb on the same chip as the main resonator.

The transmission in the circuit of Fig. 1(b) (in decibels) from rf in to rf out S_{21} is given by [16]

$$S_{21} = S_0 - 20 \lg(1 + R_0 G). \tag{4}$$

Here, S_0 is a constant and $R_0 \approx [R_L (2\pi f_0 C_2)^2]^{-1} \approx 59$ kΩ, where $R_L \approx 50\Omega$ is the line impedance. When $R_0 G_T (1 + R_0 G_T)^{-1} \Delta G/G_T \ll 1$, we may linearize Eq. (4) into

$$S_{21} = \tilde{S}_0 - \frac{20}{\ln(10)} \frac{R_0 G_T}{1 + R_0 G_T} \frac{G(V)}{G_T}, \tag{5}$$

where $\tilde{S}_0$ is another constant. For the current resonator and sensor, $R_0 G_T \approx 0.7$, i.e., the linear approximation is valid

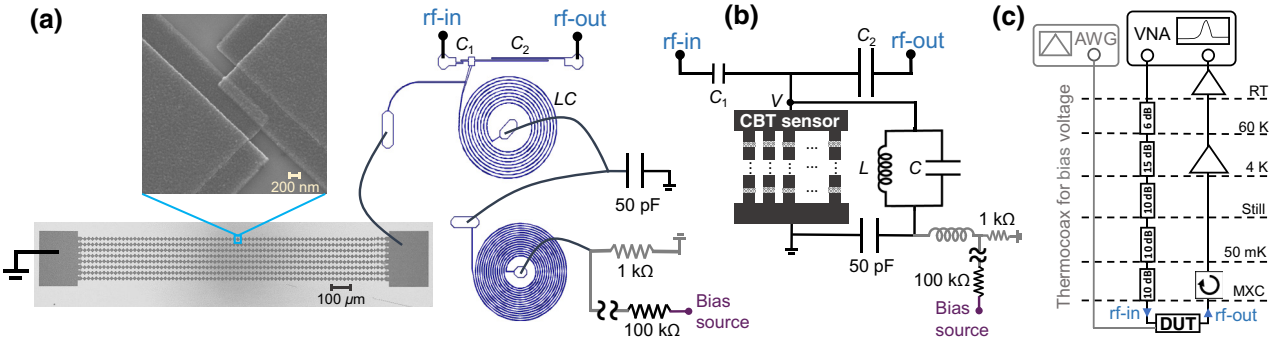

FIG. 1. The setup for rf temperature measurement. (a) The device under study (DUT) together with the resonant circuit. The CBT sensor (scanning-electron image on the left with an enlargement of one tunnel junction) forms the dissipation R of the spiral resonator (optical micrograph on the top right) in the form $R = G(v)^{-1}$, where $G(v)$ is the bias-dependent differential conductance of the junction array. $G(v)$ is obtained from the transmission S_{21} between the rf-in and rf-out ports, via the coupling capacitors C_1 and C_2, respectively. The dc bias across the CBT array is applied via an on-chip bias tee formed of another superconducting spiral inductor on the bottom right. Physically, the CBT is on one chip and the rest of the components are on another one, apart from the 100-kΩ bias resistor at room temperature and the 1-kΩ one and the 50-fF capacitor off the chip on the sample holder. The spiral resonators are made out of Nb. (b) The equivalent circuit of panel (a). (c) The experimental rf setup for the CBT measurement outside the sample stage, including the low-temperature and room-temperature components.

for all temperatures here, i.e., for $\Delta G/G_T \ll 1$. Secondary temperature measurements at zero bias, i.e., measurements of $\Delta G/G_T$ without a bias sweep, are certainly possible as well, since the grounding of the sensor at the base temperature gives extra stability to the biasing [16]. Due to the focus on primary thermometry, we do not present data on secondary measurements.

IV. DESCRIPTION OF THE EXPERIMENT

In this work, we present a simultaneous measurement of three different CBT sensors in a dilution refrigerator in the temperature range around 200 mK. One of the sensors, coined sample CBT100, is a reference consisting of chains of 100 junctions in each with ten parallel arrays. This CBT is made of Al and Cu, with superconductivity suppressed by the imposed field of a permanent magnet. It has large-volume interjunction islands to ensure proper thermalization. It has been proved to provide accurate temperature in numerous earlier experiments in the range 10–500 mK [7]. This sensor is measured using standard lock-in techniques to obtain the differential conductance at low frequency (approximately 30 Hz).

The other two CBT sensors (CBT80) are made of Al-Mn alloy to avoid superconductivity in the absence of a magnetic field down to the lowest temperatures [19]. The sample CBT80-dc is again connected to a low-frequency lock-in circuit to measure the differential conductance. This serves as another reference sample for the main device of the current work, sample CBT80-rf, which is the sensor connected to the rf circuitry described above and shown in Fig. 1(a). These two latter sensors are made in the same fabrication batch with nominally identical characteristics. The CBT80-dc and CBT80-rf devices are fabricated on an oxidized Si substrate by two-angle shadow evaporation through a suspended germanium hard mask [20] that is patterned by electron-beam lithography. The devices are deposited in an electron-beam evaporator using an alloy target with a 0.3% nominal Mn concentration. First, an approximately 20-nm-thick film is evaporated (30 nm deposited at -45° tilt angle) at a rate of 3 Å/s, followed by *in situ* oxidation in 10-mbar pure oxygen for 10 min. The tunnel junctions are completed by depositing the approximately 30-nm-thick second electrode (40 nm at $+45^\circ$ tilt angle). The overlap area of each junction is approximately 1.2 μm $\times$ 180 nm. The lateral size of the island between neighboring junctions is 15 μm $\times$ 15 μm. This relatively small island size and the weak electron-phonon coupling in the Al-Mn alloys [21,22] limit the electron thermalization at temperatures below 200 mK; hence we present experiments only above this range.

The CBT80-rf connects in parallel to a superconducting spiral resonator. The resonator is made of sputtered 200-nm Nb film on a 675 μm-thick high-resistance intrinsic silicon wafer and patterned by electron-beam lithography and a reactive-ion-etching process. For the reading out the transmittance, the resonator is capacitively coupled to the input (output) microwave feed-lines as shown in Figs. 1(a) and 1(b) and could easily be integrated with an on-chip bias tee and a divider on the sample holder. The sample is voltage biased by a triangular waveform at 5 Hz from an arbitrary waveform generator (AWG) at room temperature through a thermocoax line to a 1 kΩ surface-mount load resistor grounded on the sample holder. It is also connected in parallel with the CBT80-rf via the spiral coil of the on-chip bias tee. The incident microwave signal comes via several attenuators distributed at varying temperatures in order to minimize the thermal noise from high temperatures before exciting the resonator. The coupled output voltage across the resonator is amplified by the high-electron-mobility transistor amplifier at 4 K and a circulator with a bandwidth between 480 MHz and 720 MHz, which isolates the sample from the amplifier noise by 20 dB. The signal is amplified again at room temperature to ensure that it well exceeds the noise floor of the vector network analyzer (VNA).

The change of the conductance of the CBT80-rf by the bias voltage is then reflected in the height and width of the transmittance peak. The fast measurement is done by biasing the CBT80-rf with a triangular waveform with a peak-to-peak voltage of 60 mV, using the AWG and monitoring the transmittance at resonant frequency f_0 by a VNA with an intermediate frequency bandwidth of 1 kHz. The corresponding sampling time interval is 1.08 ms. The data acquisition is synchronized with the triangular waveform through a transistor-transistor logic trigger from the AWG to the VNA, with a rising trigger repeating each 10 s.

V. RESULTS

Figure 2 demonstrates the key feature of the measurement, namely that there is no significant difference between the CBT80-dc and CBT80-rf curves: the low-frequency and rf measurements then yield essentially the same temperature. The shoulder shapes are slightly different in the reference (CBT100-dc) and CBT80 samples. This is because of the nonoptimized sensor design of the Al-Mn samples (CBT80-dc and CBT80-rf), i.e., the thermalization is limited by the smallness of the islands in between the junctions.

Figure 3(a) shows ten successive transmission curves taken in 1 s with the said triangular wave pattern, as indicated by the light-gray line in the figure. The widths of these peaks in S_{21} then serve as the thermometer based on Eqs. (1) and (5). The temperature is obtained by finding the best fit of the form given by these equations for each half period of the triangular drive and determining the full width at half maximum for each curve. Figure 3(b) shows the temperatures extracted from such fits for 100 successive peaks, with alternative polarity of the linear

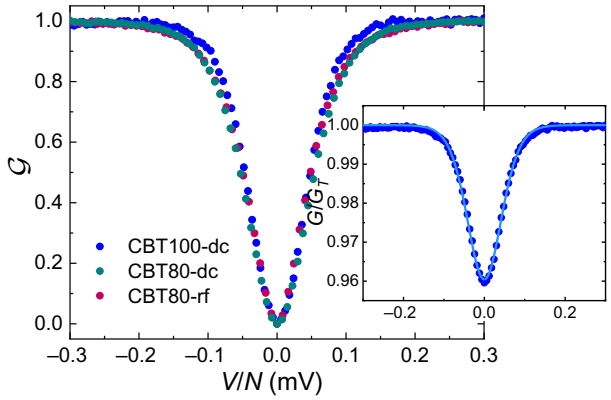

FIG. 2. The results of the conductance measurements of the three sensors at $T \sim 208$ mK versus the voltage per junction, V/N. For convenient comparison, the conductance has been normalized to the range 0–1 by presenting $\mathcal{G} \equiv [G(V) - G(0)]/[G_T - G(0)]$. All the dips have approximately the same width and shape. The reference-sensor (CBT100) data are shown by symbols as $G(V)/G_T$ separately in the inset with a fit (line) from Eq. (1), yielding $u = E_C/(k_B T) \sim 0.24$ for this measurement.

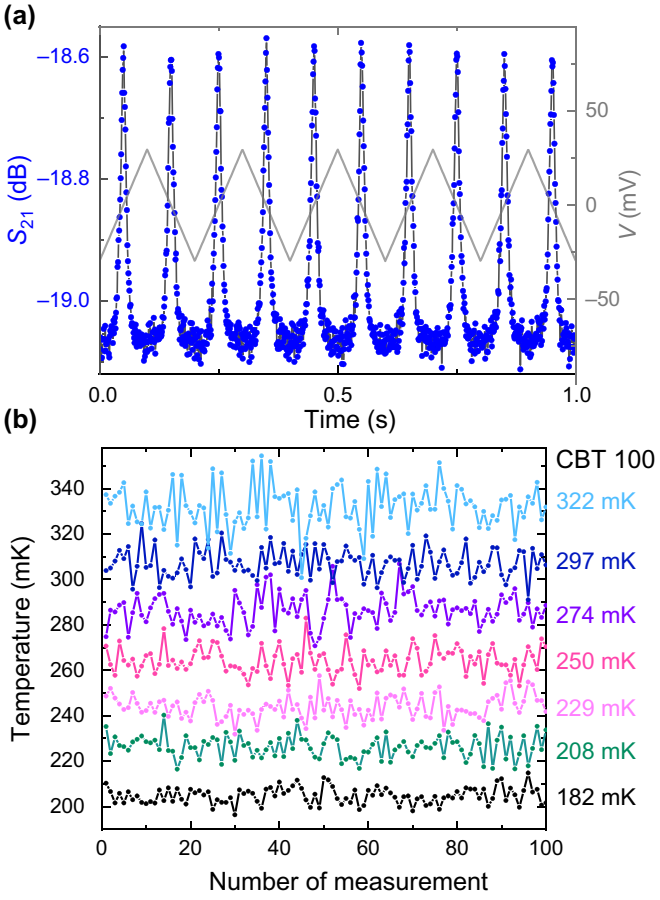

FIG. 3. Transmission S_{21} measurements. (a) S_{21} using a symmetric triangular voltage ramp in the range ± 30 mV across the array, repeating a half-period ramp each 100 ms, measured at $T = 182$ mK. Successive peaks then correspond to opposite ramp directions. S_{21} inverts the conductance dip [see Eq. (5)]. (b) T determined at each measurement temperature (reference temperatures from CBT100-dc are indicated for each set of data on the right) from 100 peaks of the type in the top panel repeated once in 100 ms. From these sets, we deduce a noise-equivalent temperature NET (see text) in the absolute (full-curve) measurement ranging from NET $= 1 \cdots 3$ mK$/\sqrt{\text{Hz}}$ from the lowest (200 mK) to the highest (340 mK) temperatures.

sweep of V. At each bath temperature, indicated by the reference CBT100-dc thermometer reading on the right-hand side, the sequence of temperatures indicates some scatter in this fast measurement. We achieve a noise-equivalent temperature NET of approximately 1 mK$/\sqrt{\text{Hz}}$ (a 1-sigma uncertainty of 2% at the bath temperature of 200 mK in 100 ms). The value of NET is obtained as the square root of the quantity found by multiplying the variance of T for the 100 points in Fig. 3 at each temperature by the measurement time (100 ms here). The operating time of 100 ms is a 1000-fold improvement as compared to standard methods with measurement times in minutes in lock-in or direct dc detection.

VI. DISCUSSION

In this work, we demonstrate an efficient way to measure subkelvin absolute temperatures by a Coulomb-blockade thermometer coupled to a superconducting resonator. We envision some future improvements to the method, both from the point of view of low-temperature circuitry and room-temperature instrumentation.

In order to increase the signal-to-noise ratio, some sources of noise can be suppressed by standard means. First, in our device, the coupling with the resonator is made with simple capacitors forming first-order high-pass filters; the noise can be reduced further using a more complex circuitry for selective coupling, reducing the bandwidth, or increasing the order. Apart from the sample, the noise can also be controlled by the choice of the circuitry in the cryostat; in our experiment, a single large-bandwidth circulator is used between the sample and the 4-K HEMT amplifier. Its purpose is to protect the sample from the back-action noise of the amplifier; it can be improved with a more selective circulator and/or by adding a second one with an additional 20 dB rejection. Ultimately, the use of a low-temperature amplifier, such as the Josephson parametric amplifier, should significantly reduce this noise; however, it would also increase the complexity of the circuit.

Most of the room-temperature electronics can be packed in a complex single chip for easy-to-use commercial purposes. Here, we use general-purpose instruments but only a few features of them are really used. First, a clock is needed for synchronization; both a low-frequency triangular and a high-frequency sinusoidal generator rely

on it. Moreover, working with telecommunication frequencies, specific purpose integrated circuits exist to perform demodulation and, finally, a regular field-programmable gate array can be programmed to extract the temperature as described in the text. We present here a proof-of-concept technique for Coulomb-blockade thermometry that will hopefully find applications in both basic science as well as practical instruments.

ACKNOWLEDGMENTS

This work was supported by Academy of Finland Grant No. 312057 (QTF Centre of Excellence) and by the European Metrology Programme for Innovation and Research (EMPIR) program co-financed by the Participating States and by the European Union Horizon 2020 research and innovation program. We acknowledge the provision of facilities and technical support by Aalto University at the OtaNano—Micronova Nanofabrication Center and through the low temperature laboratory (LTL) infrastructure, which is part of the EU Horizon 2020 European Microkelvin Platform (EMP), No. 824109.

[1] D. V. Averin and K. K. Likharev, in *Mesoscopic Phenomena in Solids*, edited by B. L. Altshuler, P. A. Lee, and R. A. Webb (Elsevier, Amsterdam, 1991), p. 173.

[2] G. L. Ingold and Y. V. Nazarov, in *Single Charge Tunneling*, edited by H. Grabert and M. H. Devoret (Plenum Press, New York, 1992), p. 21.

[3] J. P. Pekola, K. P. Hirvi, J. P. Kauppinen, and M. A. Paalanen, Thermometry by Arrays of Tunnel Junctions, Phys. Rev. Lett. **73**, 2903 (1994).

[4] S. Farhangfar, K. P. Hirvi, J. P. Kauppinen, J. P. Pekola, J. J. Toppari, D. V. Averin, and A. N. Korotkov, One dimensional arrays and solitary tunnel junctions in the weak Coulomb blockade regime: CBT thermometry, J. Low Temp. Phys. **108**, 191 (1997).

[5] T. Bergsten, T. Claeson, and P. Delsing, A fast, primary Coulomb blockade thermometer, Appl. Phys. Lett. **78**, 1264 (2001).

[6] N. Yurttagül, M. Sarsby, and A. Geresdi, Indium as a High-Cooling-Power Nuclear Refrigerant for Quantum Nanoelectronics, Phys. Rev. Appl. **12**, 011005 (2019).

[7] O. M. Hahtela, A. Kemppinen, J. Lehtinen, A. J. Manninen, E. Mykkänen, M. Prunnila, N. Yurttagül, F. Blanchet, M. Gramich, B. Karimi, and E. T. Mannila, Coulomb Blockade Thermometry on a Wide Temperature Range, 2020 Conference on Precision Electromagnetic Measurements (CPEM) (2020).

[8] M. Sarsby, N. Yurttagül, and A. Geresdi, 500 microkelvin nanoelectronics, Nat. Commun. **11**, 1492 (2020).

[9] M. Palma, C. P. Scheller, D. Maradan, A. V. Feshchenko, M. Meschke, and D. M. Zumbühl, On-and-off chip cooling of a Coulomb blockade thermometer down to 2.8 mK, Appl. Phys. Lett. **111**, 253105 (2017).

[10] D. Bradley, R. George, D. Gunnarsson, R. P. Haley, H. Heikkinen, Yu. A. Pashkin, J. Penttilä, J. R. Prance, M. Prunnila, L. Roschier, and M. Sarsby, Nanoelectronic primary thermometry below 4 mK, Nat. Commun. **7**, 10455 (2016).

[11] M. Meschke, A. Kemppinen, and J. P. Pekola, Accurate Coulomb blockade thermometry up to 60 kelvin, Phil. Trans. R. Soc. A **374**, 20150052 (2016).

[12] A. T. Jones, C. P. Scheller, J. R. Prance, Y. B. Kalyoncu, D. M. Zumbühl, and R. P. Haley, Progress in cooling nanoelectronic devices to ultra-low temperatures, J. Low Temp. Phys. **201**, 772 (2020).

[13] M. Samani, C. P. Scheller, N. Yurttagül, K. Grigoras, D. Gunnarsson, O. S. Sedeh, A. T. Jones, J. R. Prance, R. P. Haley, M. Prunnila, and D. M. Zumbühl, Microkelvin electronics on a pulse-tube cryostat with a gate Coulomb blockade thermometer, ArXiv:2110.06293.

[14] J. P. Pekola, J. J. Toppari, J. P. Kauppinen, K. M. Kinnunen, and A. J. Manninen, Coulomb blockade-based nanothermometry in strong magnetic fields, J. Appl. Phys. **83**, 5582 (1998).

[15] D. R. Schmidt, C. S. Yung, and A. N. Cleland, Nanoscale radio-frequency thermometry, Appl. Phys. Lett. **83**, 1002 (2003).

[16] B. Karimi and J. P. Pekola, Noninvasive Thermometer Based on the Zero-Bias Anomaly of a Superconducting Junction for Ultrasensitive Calorimetry, Phys. Rev. Appl. **10**, 054048 (2018).

[17] J. M. A. Chawner, S. Barraud, M. F. Gonzalez-Zalba, S. Holt, E. A. Laird, Yu. A. Pashkin, and J. R. Prance, Nongalvanic Calibration and Operation of a Quantum Dot Thermometer, Phys. Rev. Appl. **15**, 034044 (2021).

[18] I. Ahmed, A. Chatterjee, S. Barraud, J. J. L. Morton, J. A. Haigh, and M. Fernando Gonzalez-Zalba, Primary thermometry of a single reservoir using cyclic electron tunneling to a quantum dot, Commun. Phys. **1**, 66 (2018).

[19] S. T. Ruggiero, A. Williams, W. H. Rippard, A. Clark, S. W. Deiker, L. R. Vale, and J. N. Ruggiero, Dilute Al-Mn alloys for low-temperature device applications, J. Low Temp. Phys. **134**, 973 (2004).

[20] J. P. Pekola, O.-P. Saira, V. F. Maisi, A. Kemppinen, M. Möttönen, Y. A. Pashkin, and D. V. Averin, Single-electron current sources: Toward a refined definition of the ampere, Rev. Mod. Phys. **85**, 1421 (2013).

[21] L. J. Taskinen and I. J. Maasilta, Improving the performance of hot-electron bolometers and solid state coolers with disordered alloys, Appl. Phys. Lett. **89**, 143511 (2006).

[22] L. J. Taskinen, J. T. Karvonen, and I. J. Maasilta, Electron-phonon interaction in a thin Al-Mn film, Nucl. Instrum. Methods Phys. Res. A **559**, 639 (2006).

[23] J. P. Pekola, J. K. Suoknuuti, J. P. Kauppinen, M. Weiss, P. v. d. Linden, and A. G. M. Jansen, Coulomb blockade thermometry in the milli-kelvin temperature range in high magnetic fields, J. Low Temp. Phys. **167**, 263 (2002).